# Barrier transmission map of one-dimensional nonlinear split-ring-resonator-based metamaterials: Bright, dark, and gray soliton resonances

Arthur R. McGurn*
*Department of Physics, Western Michigan University, Kalamazoo, MI 49008-5252, USA*
(Received 4 June 2013; published 8 October 2013)

The barrier transmission characteristics of a one-dimensional chain of optically linear split-ring resonators (SRRs) containing a barrier composed of optically nonlinear split-ring resonators are studied. (This is an analogy to the quantum mechanical problem of the resonant transmission of a particle through a finite barrier potential.) The SRRs are idealized as inductor-resistor-capacitor-equivalent resonator circuits where the capacitance is either from a linear dielectric medium (optically linear SRRs) or from a Kerr-type nonlinear dielectric medium (optically nonlinear SRRs). The SRRs are arrayed in a one-dimensional chain and interact with one another through weak nearest-neighbor mutually inductive couplings. The transmission maxima of the SRR barrier problem are studied as they are located in a two-dimensional parameter space characterizing the linear mutually inductive coupling and the nonlinear Kerr dielectric of the SRRs of the barrier. The result is a two-dimensional map giving the conditions for the existence of the resonant-barrier modes that are excited in the transmission process. The various lines of transmission maxima in the two-dimensional plot are associated with different types of resonant excitations in the barrier. The map is similar to one recently made in McGurn [Phys. Rev. B **77**, 115105 (2008)] for the resonant-transmission modes of a nonlinear barrier in a photonic crystal waveguide. The SRR problem, however, is quite different from the photonic crystal problem as the nonlinear difference equations of the two systems are different in the nature of their nonlinear interactions. Consequently, the results for the two systems are briefly compared. The transmission maxima of the SRR system occur along lines in the two-dimensional plot, which are associated with modes resonantly excited in the barrier. These lines of resonant modes either originate as a simple evolution from the resonant modes of the linear barrier limit or as lines of soliton breather modes of the bright, dark, or gray types. The soliton modes arise either spontaneously at a lower critical value of the nonlinearity of the barrier media or from the breakup of a barrier mode in the linear media limit as the barrier media become increasingly nonlinear. The soliton resonances are identified by comparing the wave functions and energies of the barrier excitations with those of solitons in an infinite chain composed of barrier material. Results for the infinite chain in Giri, Choudhary, Gupta, Bandyopadhyay, and McGurn [Phys. Rev. B **84**, 155429 (2011)] for bright solitons are used for this identification, and in the Appendix we present additional solutions for dark and gray solitons that were not included in our previous treatments.

DOI: 10.1103/PhysRevB.88.155110 PACS number(s): 05.45.Yv, 78.67.Pt, 81.05.Xj, 42.65.−k

## I. INTRODUCTION

Recently there has been much interest in split-ring-resonator-(SRR)-based metamaterials.[1–16] These are artificial (engineered) nanomaterials that are capable of exhibiting optical properties not found in nature. They form the basis of the design of many types of negative refractive media[1–3,17] and cloaking devices.[1–3,18,19] Metamaterials are formed by the periodic repetition of SRRs in a medium exhibiting an effectively uniform dielectric response. The SRRs are used to tune the frequency-dependent magnetic response of the metamaterial[1–3] at wavelengths that are much larger than the lattice constant of the lattice of SRRs. Typically the SRR are designed to have permeability resonances at THz frequencies and below, where such frequency resonances do not occur in natural (nonengineered) materials. These resonances give rise to the technological important properties of metamaterials.[1–16]

In addition to their important technological properties, metamaterials have been studied for their interesting excitations.[4–16] These include simple wavelike excitations associated with the permeability resonances in optically linear systems[6–9] and, in optically nonlinear systems,[4,5,10–14,20] a wide variety of different types of soliton excitations dependent on optical nonlinearity for their existence. The excitation modes in linear SRR-based metamaterials are known as magneto-inductive waves.[6,7] In nonlinear SRR-based metamaterials, additional bright soliton and dark soliton inductive modes are found[4,5,15,20] and, as we shall show later, a class of gray solitons.

There have been many designs proposed for SRRs,[21] but a common idealized feature is a ring-shaped structure that is split so that a gap occurs in the ring. The resulting component is described theoretically as an equivalent inductor-resistor-capacitor (IRC) circuit.[4,5,15,20] The self-inductance comes from the ring, the resistance comes from the wire of the ring and from small radiation losses, and the ring gap containing a dielectric medium provides a capacitance. If the material in the ring gap is linear dielectric medium, the SRR gives a linear response, but if the gap material is Kerr nonlinear medium,[4,5,10,11,20] the SRR gives a nonlinear response. In this paper, we will follow Refs. 4,15, and 20 in studying a one-dimensional array of simple SRRs. These are formed as rings that are split by a simple gap. The SSRs are then coupled to one another by a weak mutual inductance. This should allow for a semiquantitative discussion of the phenomena accessible to many of the more detailed experimental realizations of such systems as well as to realizations of the simple system itself.[4–9]

In this paper, we treat a chain of linear media SRR containing a barrier of nonlinear media SRR.[21–24] (Note:

 

In the remainder of the paper the "chain of linear media" means that the capacitor splits or gaps in its SRR are filled with a linear dielectric media, and the "barrier of nonlinear media" means that the capacitor splits or the gaps in its SRR are filled with a Kerr nonlinear dielectric medium. The nonlinearity comes from the material in the split or gap of the SRR and, as mentioned in past studies, it has little effect on the mutually inductive couplings, which are linear.) The scattering transmission through the barrier is studied, and the transmission maxima through the nonlinear barrier are mapped out in a two-dimensional space of the linear mutually inductive coupling between nearest-neighbor barrier sites and a parameter characterizing the Kerr nonlinearity of the SRR of the barrier. These maxima arise from the resonant excitations in the barrier of modified modes of the linear system and soliton modes of the bright, dark, and gray type. A focus of the paper is on the lines in this two-dimensional plot that arise from the resonant excitation of bright, dark, and gray solitons in the barrier. The identification of these lines of resonances is made using the solutions for the soliton types in a uniform infinite chain composed only of barrier material.

A similar map was studied by us for a photonic crystal waveguide containing a barrier composed of Kerr nonlinear media, and the soliton solutions in this map were identified.[22–24] It is interesting to compare the results of the photonic crystal systems with that studied in this paper. The photonic crystal system contains both onsite nonlinearity and nonlinearity in the coupling between the sites. The SRR system contains only onsite nonlinearity, and this gives qualitative differences between the two systems.

A second focus of the paper is the presentation of soliton solutions for the dark and gray soliton modes of a uniform infinite nonlinear chain and a discussion of their continuum limit forms. These were not treated in our recent publication on solitons in these systems.[20]

The order of the paper is as follows. In Sec. II, the theory of the SRR chain and barrier is presented, and the results and discussions are presented in Sec. III. An Appendix section presents solutions of the bright, dark, and gray solitons and their continuum limit forms, which are quoted in the body of the text. Section IV presents conclusions.

## II. THEORETICAL DEVELOPMENT

### A. The chain and its discrete and continuum models

We consider the one-dimensional model of weakly coupled SRRs treated in Ref. 20 (see Fig. 1). It is similar to that considered by Eleftheriou *et al.*[4,5,15,25] The system consists

X X X O O O O O O O O O X X X

X=Linear Dielectric in Gap

O=Nonlinear Dielectric in Gap

FIG. 1. Schematic of an infinite chain of inductively coupled SRR containing a barrier. The X represents an SRR with linear dielectric media in its gap, and the O represents an SRR with nonlinear dielectric media in its gap. The sites of the chain are labeled consecutively by integers, and in the figure only a finite portion of the chain containing the barrier is shown.

of metal rings of self-inductance, $L$, that are split with a gap containing a dielectric material, which may be either optically nonlinear of the form $\varepsilon(|E|^2)=\varepsilon_0(\varepsilon_l+\alpha\frac{|E|^2}{E_c^2})$, where $\alpha=\pm1$ and $E_c$ is a characteristic (large) electric field or optically linear with $\alpha=0$. Each SRR forms an IRC circuit with a time-varying current and capacitive charge. The metamaterial array is formed by taking the SRR as basis elements on a one-dimensional Bravais lattice of lattice constant, $d$, interacting by weak nearest-neighbor inductive couplings, and the SRRs are labeled consecutively along the chain by integers, $n$. In Ref. 4, it was found that the mutually inductive couplings, $M$, in our system are $M>0$ for SRR with a common axis perpendicular to their planes, and $M<0$ for coplanar SRR. This can be roughly understood by applying Lenz's law to two such rings.

The equations of motion for the capacitive charge on the SRRs of a uniform infinite chain, in the notation of Ref. 20, are given by

$$\ddot{q}_n+\lambda_c(\ddot{q}_{n+1}+\ddot{q}_{n-1})+q_n-\left(\frac{\alpha}{\varepsilon_l}\right)q_n^3=0. \tag{1}$$

Here $\lambda_c=\frac{M}{L}$, $q_n=\frac{Q_n}{Q_c}$, and $Q_n$ are the charge on the gap of the $n$th SRR, and $Q_c=C_lU_c$, $U_c=d_gE_c$, and $C_l=\varepsilon_0\varepsilon_l(A/d_g)$, where $d_g$ and $A$ are the width and area of the SRR gaps, $\ddot{q}_n=\frac{d^2q_n}{d\tau^2}$, and $\tau=t_0\omega_l$ for $\omega_l=\frac{1}{\sqrt{LC_l}}$ is the dimensionless time. (Note: Here the time $t_0$ is the same as that denoted $t$ in Eq. 6 of Ref. 20.) In the discussions of a chain containing a barrier, which are the subject of this paper, the chain equation [i.e., Eq. (1)] is modified to include a finite-length barrier segment in which $\lambda_c=\lambda$ is changed to a new value $\lambda'$. This is done by changing the mutual induction between the SRR in the barrier region.

To understand the barrier results, it is also useful to consider two continuum-limiting forms of Eq. (1). These were obtained in Ref. 20. The continuum limits are useful for studying solutions that are slowly varying in space and are obtained by making the expansion $\ddot{q}_{n\pm1}=[\ddot{q}\pm d\frac{\partial\ddot{q}}{\partial x}+\frac{1}{2}d^2\frac{\partial^2\ddot{q}}{\partial x^2}+\cdots]_{x=nd}$, where $q=q(x)$ is the generalized continuum variable corresponding to $q_l$. A first continuum form, given within the context of the rotating wave approximation (RWA), for modes of frequency $\omega$ with arbitrary amplitudes and having wave functions that are separable in space and time coordinates is

$$\omega^2\lambda_c\frac{\partial^2q}{\partial x^2}-[1-(1+2\lambda_c)\omega^2]q+\frac{3\alpha}{\varepsilon_l}|q|^2q=0. \tag{2}$$

Here $x$ is rescaled to be measured in units of the lattice constant $d$ (i.e., $x/d\to x$). A second continuum form of Eq. (1), again within the context of the RWA, for modes of frequency $\omega$ with small amplitudes and wave functions that are nonseparable in space and time coordinates is also obtained. For $|\lambda_c|\ll1$, these modes are described by the nonlinear Klein-Gordon equation[20]

$$\frac{\partial^2q}{\partial\tau^2}-ab\frac{\partial^2q}{\partial x^2}+b\left[q-\frac{\alpha}{\varepsilon_l}q^3\right]=0, \tag{3}$$

where $a=\lambda_c/(1+2\lambda_c)$ and $b=1/(1+2\lambda_c)$. Here $x$ is again rescaled to be expressed in units of $d$ (i.e., $x/d\to x$). In Ref. 20, the nonlinear Schrodinger formulation, which has been commonly used in studies of the SRR chain,[4,15] was

shown to be an approximation to Eq. (3). A continuum limit form of Eq. (1), which does not require that $|\lambda_c| \ll 1$, was also obtained in Ref. 20 for modes with wave functions separable in the space and time coordinates, but this will not be used here.

### B. Solitons of the infinite chain

Our focus in the barrier-scattering problem is on the excitation of soliton modes in the barrier media and their effect on the transmission through the barrier.[22–24] For this, it is necessary to understand the properties of the soliton solutions that exist in a uniform infinite chain of nonlinear SRRs. In Ref. 20, a variety of solitonlike excitations that exist in the infinite SRR chain were studied using the formulations in Eqs. (1)–(3). In the case of the solutions of the discrete system of Eq. (1), bright solitons or pulselike discrete breather modes were identified. Explicit analytical forms of the solutions and conditions for their existence were given. For the continuum limit cases in Eqs. (2) and (3), a variety of stationary and mobile bright and dark soliton mode solutions were found and matched to some of the discrete solutions. A brief summary of these results is presented in the Appendix.

The Appendix also includes new results on solitonlike solutions of these systems, which were not considered in our previous work. The results include the following. For the discrete system in Eq. (1), analytical forms for the solutions of dark solitonlike discrete breather modes are given, and it is shown how the dark soliton modes of the continuum Eqs. (2) and (3) are related to these. Previously unconsidered gray soliton modes in both the discrete and continuum equations are also shown to exist.

The results for the solitonlike bright, dark, and gray modes are used in the primary text to understand the structure of the resonant-scattering transmissions observed in the barrier-scattering problem of the discrete system. The discussions of the resonant scattering are fashioned after those in Ref. 22, which treated barrier scattering in photonic crystal waveguides and its representation in a two-dimensional space of parameters describing the linear and nonlinear interactions in the waveguide barrier. As explained later, the present SRR system involves a fundamentally different set of differences equations than those treated in the photonic crystal paper and give, correspondingly, different types of results from those of the photonic waveguide systems.

### C. The barrier problem

For the discrete system based on Eq. (1), we consider the scattering modes from a barrier of nonlinear media embedded in a chain of linear media. The modes are separable in space and time coordinates with time dependence $e^{-i\omega\tau}$ and are studied within the context of the RWA. The difference equations for a system with a barrier of $m$ sites are

$$-\omega^2[q_n + \lambda(q_{n+1} + q_{n-1})] + q_n = 0 \tag{4a}$$

for $n < 0$ or $n > m + 1$ in the regions of the linear media outside the barrier, and

$$-\omega^2[q_n + \lambda'(q_{n+1} + q_{n-1})] + q_n - 3\left(\frac{\alpha}{\varepsilon_l}\right)|q_n|^2 q_n = 0 \tag{4b}$$

for $1 \leqslant n \leqslant m$ within the nonlinear barrier. Here the mutual-inductance couplings $\lambda$ and $\lambda'$ are different inside and outside the barrier and $\alpha = 0$ outside the barrier. The boundary conditions at the left edge of the barrier are

$$\ddot{q}_0 + \lambda'\ddot{q}_1 + \lambda\ddot{q}_{-1} + q_0 = 0 \tag{4c}$$

and at the right edge of the barrier

$$\ddot{q}_{m+1} + \lambda\ddot{q}_{m+2} + \lambda'\ddot{q}_m + q_{m+1} = 0. \tag{4d}$$

Note that for the constant frequency forms of Eq. (4), a symmetry is observed that is reminiscent of that between classical ferro- and antiferromagnet systems. Specifically, the equations of motion are invariant under the replacements $\lambda \to -\lambda, \lambda' \to -\lambda'$ and $q_n \to (-1)^n q_n$.

Solutions of Eq. (4) for the elastic scattering are obtained using transfer matrix techniques, taking the form

$$q_l = te^{ikl} \tag{5a}$$

to the right of the barrier for $l \geqslant m + 1$ and

$$q_l = ue^{ikl} + re^{-ikl} \tag{5b}$$

for $l \leqslant 0$ to the left of the barrier. The transmission coefficient is then $T = |\frac{t}{u}|^2$ and $0 \leqslant T \leqslant 1$. Equation (5) represents a solution in the form of a plane wave in the linear media interacting with the nonlinear barrier. As with our treatment of this solution form in the photonic crystal barrier problem studied in Ref. 22, it yields to an exact closed form solution. As in Ref. 22, due to space limitations, the equations of the full solution are not given here. It is also possible and of interest to find solutions for the system driven externally at a single site. This is a problem, however, that is beyond the scope of the present work and will be treated elsewhere.

## III. RESULTS AND DISCUSSIONS

In Fig. 2, the locations of the transmission maxima through the nonlinear barrier system are plotted as they are found in the two-dimensional space of $\frac{\alpha}{\varepsilon_l}t^2$ (characterizing the barrier nonlinearity) and $\lambda'$(characterizing the barrier nearest-neighbor couplings). For these plots, $t$ in Eq. (5a) is real, $k = 2.9$ and $\lambda = -0.02$ is taken from Ref. 20, and results are shown for barriers with $m = 5$ and $m = 9$ sites. This parameterization gives elastic scattering modes of frequency $\omega = 0.9811$. The transmission maxima are obtained by fixing the value of the nonlinearity and studying the transmission as a function of the barrier coupling. The locations of maxima with transmission coefficients greater than 0.2 are shown in the figures. The maxima occur as a result of resonant transmission through the barrier so that the barrier modes excited by the incident wave facilitate transmission through the barrier.

### A. The two-dimensional map of transmission maxima

It is seen in Figs. 2(a) and 2(b) that the systems of $m = 5$ and $m = 9$ have similar lines with branching features, and the number of branches or connecting lines in the plots increases as the number of barrier sites increases. Many resonant modes in the nonlinear system evolve as simple modifications of the resonant modes of the linear (i.e., $\frac{\alpha}{\varepsilon_l}t^2 = 0$) system, maintaining the same essential wave-function form but only

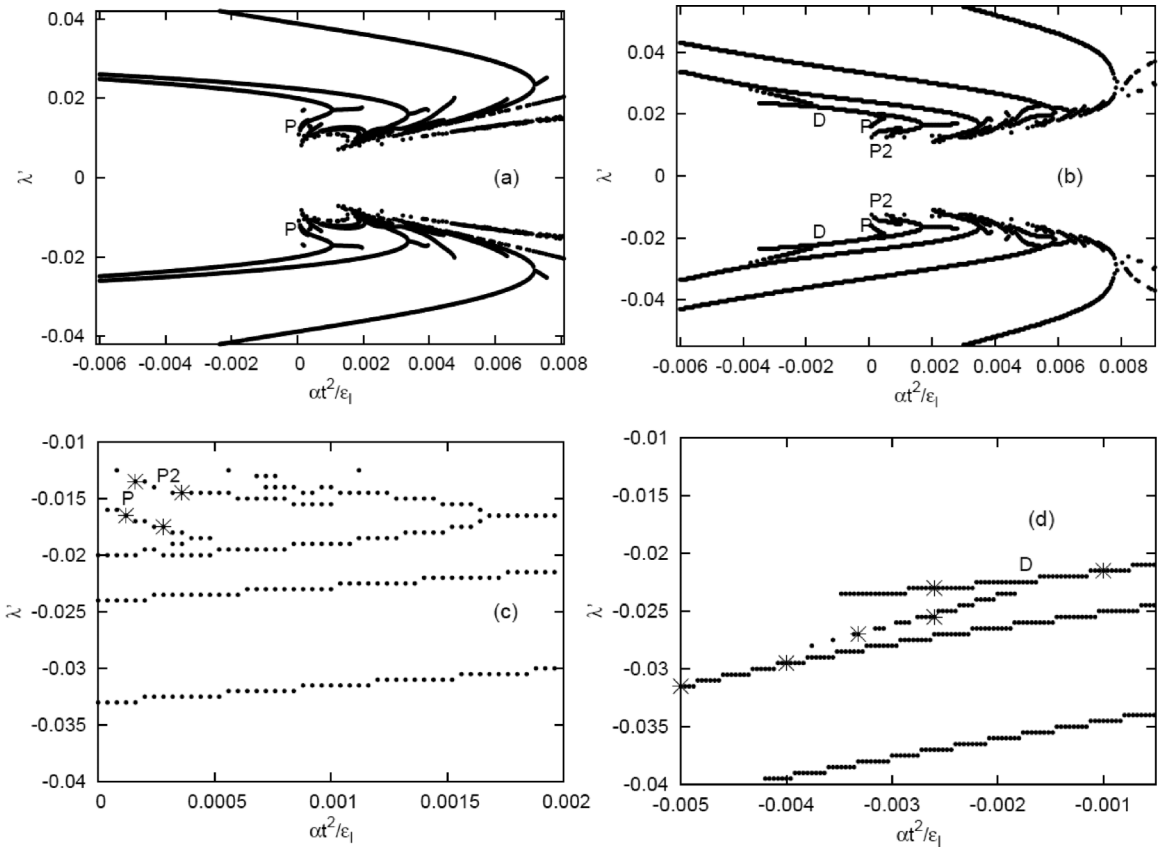


FIG. 2. Plot of the location of the barrier-transmission maxima in the $(\frac{\alpha}{\varepsilon_l}t^2,\lambda')$ plane. In the incident and transmitted linear-dielectric media $\lambda = -0.02$ and the wave number of the incident, reflected, and scattered waves is $k = 2.9$, where the lattice constant of the SRR chain is taken as unity. Results are show for (a) a system with $m = 5$ barrier sites, (b) a system with $m = 9$ barrier sites, (c) a magnification of a particular region of the plot in (b), and (d) another magnification of a particular region of the plot in (b). In these plots, the branches of bright solitons have a P to the left of them, and the branches of dark soltions have a D next to them. In (b) and (c) the branch labeled P2, passing through $(\frac{\alpha}{\varepsilon_l}t^2,\lambda') = (0.00016, -0.0135)$ and $(0.00036, -0.0145)$ contains solutions with two consecutive bright solitons resonantly excited in the barrier. In (c) and (d) some of the soliton resonances discussed in the text are emphasized on the map. Notice that in these plots the line breaks are not artifacts of the numerical methods but come from the $T > 0.2$ selection condition on the maxima.

with a renormalization of some of its specific features. This accounts for the similarity in shape of the branching line structures in systems with different numbers of barrier sites and their increasing number with increasing barrier sites.

In addition, there are lines involving sets of resonant modes that only exist in the presence of nonlinearity or that represent basic soliton modifications of the wave-function forms occurring in the linear limit. These types of modes will be our focus. They include bright, dark, and gray-type soliton modes; resonances involving these modes also display resonant-transmission maxima along lines in the $(\frac{\alpha}{\varepsilon_l}t^2,\lambda')$ plane.[22–24]

### B. Branches not containing modes of the linear system: bright solitons

As an example, in the $m = 9$ system, resonant transmission involving bright solitons are found to occur in the branch of modes passing through the points $(\frac{\alpha}{\varepsilon_l}t^2,\lambda') = (0.00012, \pm 0.0165)$ and $= (0.00028, \pm 0.0175)$ in Figs. 2(b) and 2(c) and labeled by a P in Figs. 2(b) and 2(c). This branch of modes does not include points of the $\frac{\alpha}{\varepsilon_l}t^2 = 0$ linear system and only exists in the presence of nonlinearity. That these resonances originate from bright solitons is shown by comparing the wave functions and frequencies of the barrier modes involved in the resonant transmission with the wave functions and frequencies of the solitons found in the uniform infinite nonlinear chain characterized by the same system parameters as those of the finite barrier in the scattering problem.[22–24] This comparison is now addressed.

In Fig. 3(a), barrier-wave functions are presented at $\frac{\alpha}{\varepsilon_l}t^2 = 0.00012$ and variable $\lambda'$ for several barrier modes of the scattering problem in Fig. 2(b). The primary focus of our discussion is on the soliton modes occurring at $\lambda' = \pm 0.0165$. This is the single large amplitude mode observed in the plot, with the other smaller amplitude modes being those that evolve from modes of the linear barrier system. The soliton only appears in the presence of nonlinearity because the branch labeled P does not include $\frac{\alpha}{\varepsilon_l}t^2 = 0.0$. (A similar analysis can be made of the scattering problem for $\frac{\alpha}{\varepsilon_l}t^2 = 0.00028$ and variable $\lambda'$. This yields a single large amplitude, bright soliton found at $\lambda' = \pm 0.0175$ and many smaller amplitude modes that evolve from those of the linear system.) This mode and that at $(\frac{\alpha}{\varepsilon_l}t^2,\lambda') = (0.00028, \pm 0.0175)$ are now compared with the bright soliton modes of the infinite chain.

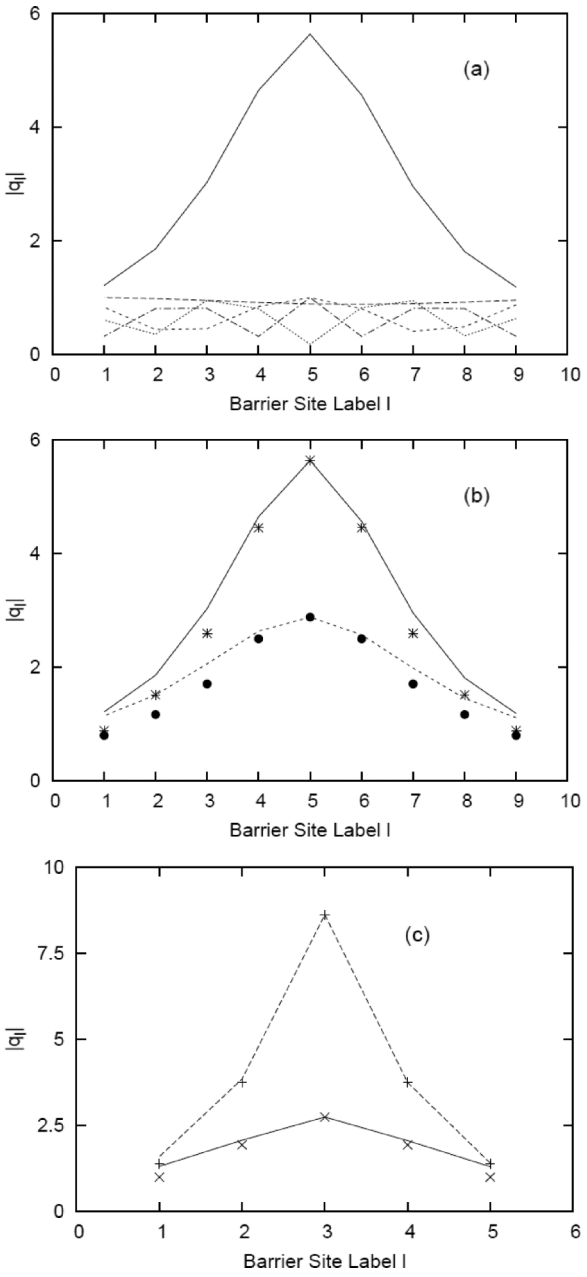


FIG. 3. Plot of the wave function amplitude of a nine-site barrier versus barrier-site number for (a) $\frac{\alpha}{\varepsilon_l}t^2 = 0.00012$ showing the pulse soliton-type mode at $\lambda' = \pm 0.0165$, which is the single mode of largest amplitude and some of the small amplitude modes that evolve from the modes of the linear system; and (b) $\frac{\alpha}{\varepsilon_l}t^2 = 0.00012$, $\lambda' = \pm 0.0165$ (upper solid) and $\frac{\alpha}{\varepsilon_l}t^2 = 0.00028$, $\lambda' = \pm 0.0175$ (lower dashed) barrier soliton-type modes. A comparison is made between the barrier modes in Fig. 3(b), and results for the uniform infinite chain-pulse solitons (discussed in Sec. A1 of the Appendix) for chain solutions with $\frac{\alpha}{\varepsilon_l} = 0.00012$, $\lambda_c = \lambda' = \pm 0.0165$, $\alpha_0 = 5.640$ (star points), and $\frac{\alpha}{\varepsilon_l} = 0.00028$, $\lambda_c = \lambda' = \pm 0.0175$, $\alpha_0 = 2.880$, (closed circle points). For the comparison, the uniform infinite chain result's $\alpha_0$ is in units of $t$ which are the units of the amplitudes in the plots. A plot is also presented in (c) for a five-site barrier at $\frac{\alpha}{\varepsilon_l}t^2 = 0.00012$, $\lambda' = \pm 0.01255$ (upper curve), and $\frac{\alpha}{\varepsilon_l}t^2 = 0.00068$, $\lambda' = \pm 0.01525$(lower curve), and the points in the plot are the corresponding results in the uniform infinite chain. Notice that in all of the plots, the system is discrete, and the lines are to guide the eye of the reader.

TABLE I. Bright stationary breather solutions of Eq. (A2) for transmission maxima points in Fig. 2.

| $\lambda_c$ | $\alpha/\varepsilon_l$ | $\alpha_0$ | $\omega$ | $q_0$ | $q_1$ | $q_2$ |
|---|---|---|---|---|---|---|
| 0.0165 | 0.00012 | 5.640 | 0.9816 | 5.640 | 4.451 | 2.594 |
| −0.0165 | 0.00012 | 5.460 | 0.9816 | 5.640 | −4.451 | 2.594 |
| 0.0175 | 0.00028 | 2.880 | 0.9817 | 2.880 | 2.497 | 1.706 |
| −0.0175 | 0.00028 | 2.880 | 0.9817 | 2.880 | −2.497 | 1.706 |

In Fig. 3(b), the barrier-wave functions and the wave functions of bright solitons in the uniform infinite nonlinear chain at $\frac{\alpha}{\varepsilon_l} = 0.00012$ (with frequency $\omega = 0.9816$) and $\frac{\alpha}{\varepsilon_l}t^2 = 0.00028$ (with frequency $\omega = 0.9817$) are presented. For the comparison, the amplitudes of the uniform infinite chain results were chosen to match the barrier resonances and to be measured in units of $t$. The agreement between the barrier and infinite-chain modes in frequency and wave functions is good and indicates that the resonant transmission arises from the excitation of soliton pulses in the barrier. Both barrier modes have much larger amplitudes than the modes that evolve from those of the linear system, and, as $\frac{\alpha}{\varepsilon_l}t^2$ increases, the bright soliton modes are found to decrease in amplitude. For this comparison, the uniform infinite chain results are obtained using Eqs. (A1)–(A2), which are explained in Sec. A1 of the Appendix. Equations (A1) and (A2) were evaluated for $(\frac{\alpha}{\varepsilon_l},\lambda') = (0.00012, \pm 0.0165)$ and $\alpha_0 = 5.64$ (the amplitude of the resonant-barrier-wave function) and for $(\frac{\alpha}{\varepsilon_l},\lambda') = (0.00028, \pm 0.0175)$ and $\alpha_0 = 2.88$ (the amplitude of the resonant-barrier-wave function), where $\alpha_0$ is taken in units of $t$ for comparison with the resonant-scattering results. For convenience, some of the results from Eqs (A1)–(A2) are also listed in Table I.

An additional related branch of transmission resonances involving bright solitons is labeled P2 in Fig. 2(b). This branch, like the P branch, also arises only in the presence of nonlinearity, but now the resonant transmission involves the excitation of two bright solitons in the barrier. More about this will be presented in a future publication.

For comparison with the results of the barrier of nine sites, Fig. 2(a) presents a plot of the transmission resonances for a barrier of five sites that is similar to that presented for the nine-site barrier. There is also a branch of bright solitons labeled P in Fig. 2(a), which does not include a $\frac{\alpha}{\varepsilon_l}t^2 = 0.0$ point of the linear system. Figure 3(c) gives a plot of the wave functions of two barrier modes of this P branch. The agreement between the barrier-wave functions and the wave functions of the uniform infinite chain are quite good. A P2 branch similar to that in Fig. 2(b), however, is absent. The five-site barrier is not long enough to support more than a single bright soliton. With this in mind, it is expected that the number of multiple bright solitons and their branches increase with increasing barrier sites. This will be discussed in a future publication.

### C. Branches of solitons originating from linear system modes: dark, gray solitons

Another source of solitons in the barrier involves the breakup of a resonant mode of the linear system as nonlinearity is introduced into the barrier. In the linear limit of the barrier,

in both $m = 5$ and $m = 9$ systems, there is a uniform mode at $(\frac{\alpha}{\varepsilon_l}t^2,\lambda') = (0.0, \pm 0.020)$ having $|q_l| = 1.0$ at each site of the barrier. As nonlinearity is introduced into the barrier media, the uniform linear barrier mode is found to evolve into dark or gray-type solitons. Behavior of this type is well known in the uniform infinite chain system, occurring as the chain goes from a linear to a nonlinear system, and should be expected in the barrier-scattering problem. We now turn to discuss the resonant scattering involving these modes.

To determine the nature of resonant-soliton scattering in the barrier, it is necessary to compare the barrier-wave functions and frequencies at resonant scattering with the wave functions and frequencies of the soliton solutions of the uniform infinite chain. An important point of comparison for these modes is the width of the mode-wave functions. While the bright solitons that we have treated earlier consist of a single intensity peak, dark and gray solitons consist of intensity dips. Both of these features are characterized by the width of the peak or dip regions.

To determine the presence of dark soliton resonances in the barrier scattering, the dark soliton solutions of the uniform infinite chain are determined in the Appendix. From these solutions, the widths of the dark solitons in the uniform infinite chain are determined as functions of $\frac{\alpha\alpha_0^2}{\lambda_c\varepsilon_l}$, and the results are presented in Fig. 4. Here $\alpha_0$, as discussed in the Appendix, is the magnitude of the asymptotic limits of the dark soliton amplitude along the chain length at infinity, and $\lambda_c$ is the coupling in the uniform infinite chain. In Fig. 4, $\alpha_0 = t$ has been taken to make a comparison with the resonances of the barrier scattering. Taking $\lambda_c = \lambda' = 0.02$ from the value of the linear-barrier-transmission maxima at $(\frac{\alpha}{\varepsilon_l}t^2,\lambda') = (0.0, \pm 0.020)$ in Fig. 2(b) and applying this to the uniform infinite chain results in Fig. 4, we find that for $\frac{\alpha\alpha_0^2}{\varepsilon_l} > 0.0033$, the dark soliton modes have a half-width of two lattice constants or less and for $\frac{\alpha\alpha_0^2}{\varepsilon_l} < 0.0033$ the dark soliton half-width rapidly increases from two lattice constants. Considering Fig. 2, this limits the regions of $(\frac{\alpha}{\varepsilon_l}t^2,\lambda')$ in which dark solitons in the barrier are expected as a resonant-scattering

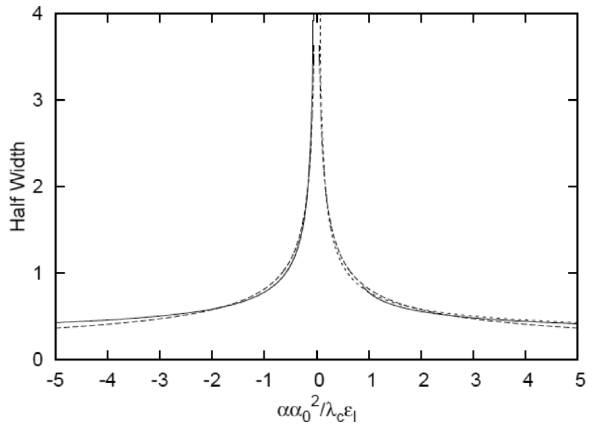


FIG. 4. Plot of the half-width in units of the lattice constant of the dark soliton versus $\frac{\alpha\alpha_0^2}{\lambda_c\varepsilon_l}$. Results from the solution in Eq. (A7) are the solid (short dashed) lines for the upper (lower) signs in Eq. (A7), and the longer dashed lines are from the continuum limit form in Eq. (A16).

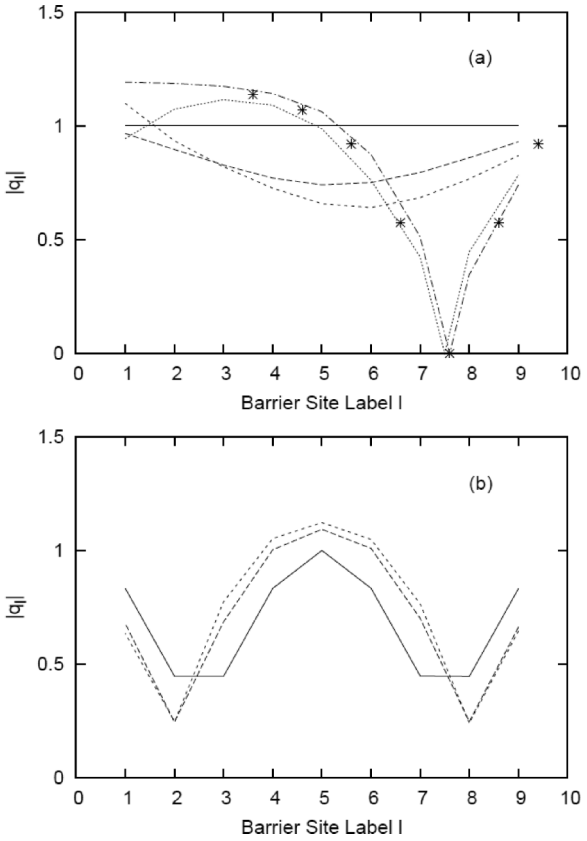


FIG. 5. Plot of $|q_l|$ versus the barrier site number for (a) barrier of nine sites at $(\frac{\alpha}{\varepsilon_l}t^2,\lambda') = (0.0, -0.020)$, $(-0.001, -0.0215)$, $(-0.0026, -0.023)$, $(-0.0026, -0.0255)$, and $(-0.00332, -0.0270)$ going in the plot from top to bottom at site number 8. For comparison with the $(-0.00332, -0.0270)$ transmission results, points for the infinite chain dark soliton evaluated at $(\frac{\alpha}{\varepsilon_l},\lambda_c) = (-0.00332, 0.0270)$ and $\alpha_0 = 1.19$ (in units of $t$ which are the units of the amplitudes in the plots) are presented on the plot. Notice that the points of the infinite chain results have been shifted along the lattice in order to make a comparison. (b) Barrier of nine sites at $(\frac{\alpha}{\varepsilon_l}t^2,\lambda') = (0.0, -0.024)$, $(-0.004, -0.0295)$, and $(-0.005, -0.0315)$ going in the plot from bottom to top at site number 5. Notice that in all of the plots, the system is discrete, and the lines passing though the discrete points in the plot are only meant as a visual aid to the reader.

mechanism. In particular, only modes for which $\frac{\alpha\alpha_0^2}{\varepsilon_l} > 0.0033$ effectively fit within barriers for which $m = 5$ or $m = 9$ and can be observed as dark soliton resonances.

### *1. Breakup into dark solitons*

We now consider the nature of the dark soliton excitations, which evolve from the $(\frac{\alpha}{\varepsilon_l}t^2,\lambda') = (0.0, -0.020)$ uniform mode of the linear barrier system. For this, the wave functions of dark solitons in the infinite chain and their widths (presented in Table II and Fig. 4, respectively) are necessary. In making the comparison of the two results, unless otherwise stated, we take the wave functions of the uniform infinite chain at infinity to approach the amplitude of the wave transmitted by the barrier, i.e., $\frac{\alpha_0}{t} = 1$.

Dark soliton resonances in the barrier of nine sites are observed in a line of modes that connects the two lines arising

TABLE II. Dark stationary breather solutions of Eq. (A7) for transmission maxima points in Fig. 2.

| $\lambda_c$ | $\alpha/\varepsilon_l$ | $\omega$ | $q_0$ | $q_1$ | $q_2$ | $q_3$ |
|---|---|---|---|---|---|---|
| 0.0255 | −0.00260 | 0.9792 | 0.0000 | 0.3677 | 0.6382 | 0.7929 |
| 0.0270 | −0.00332 | 0.9789 | 0.0000 | 0.4068 | 0.6883 | 0.8362 |
| 0.0295 | −0.00400 | 0.9776 | 0.0000 | 0.4277 | 0.7133 | 0.8564 |
| 0.0315 | −0.00500 | 0.9772 | 0.0000 | 0.4624 | 0.7515 | 0.8853 |

from the $(\frac{\alpha}{\varepsilon_l}t^2,\lambda') = (-0.00, -0.02)$ and $(-0.00, -0.024)$ linear-barrier modes. This branching is labeled D in Fig. 2(b), and it only exists in the presence of nonlinearity. It connects between two lines arising from the linear-barrier limit. In Fig. 5(a), the wave-function amplitudes of two dark soliton modes, $(\frac{\alpha}{\varepsilon_l}t^2,\lambda') = (-0.0026, -0.0255)$ and $(-0.00332, -0.0270)$, along this connecting branch are shown. The position of these modes in the two-dimensional plot of transmission maxima is indicated in the enlargement presented in Fig. 2(d). The widths of these modes agree with the results 2.56 and 2.32 from Fig. 4, and the wave functions listed in Table II are in reasonable agreement with those in Fig. 5(a) when an account is made for the shift of the modes along the barrier sites. For a comparison, results for the infinite-chain dark soliton corresponding to the $(-0.00332, -0.0270)$ transmission resonance are shown as points on the plot. Taking into account the resonant nature of the barrier mode, there is a reasonable agreement between the two modes.

Results for some modes on the line arising from $(\frac{\alpha}{\varepsilon_l}t^2,\lambda') = (-0.00, -0.02)$, but not on the connecting branch, are presented for comparison. These are modes at $(\frac{\alpha}{\varepsilon_l}t^2,\lambda') = (-0.001, -0.0215)$ and $(-0.0026, -0.023)$ and indicate the beginnings of a breakup of the uniform mode, which is only accomplished in the line of modes that branches off from them. This shows that the branch of dark soliton modes arises from the breakup of the uniform amplitude linear mode as the nonlinearity enters and increases in the system.

In Fig. 5(b), we look at the wave-function amplitudes of the resonances at the linkage point of the dark soliton resonant branch with the line of modes that evolve from the $(\frac{\alpha}{\varepsilon_l}t^2,\lambda') = (-0.00, -0.024)$ linear mode. The $(\frac{\alpha}{\varepsilon_l}t^2,\lambda') =$

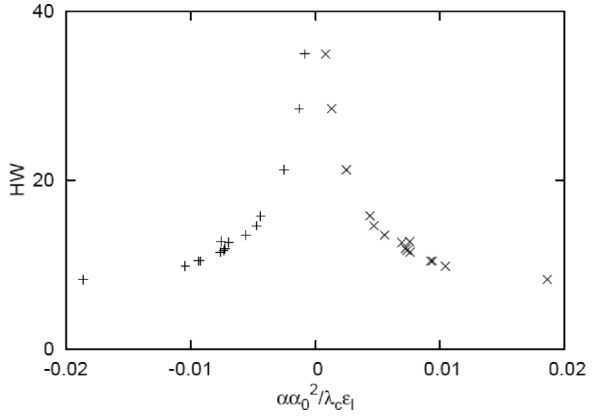


FIG. 6. Gray soliton half-width, $HW$, versus $\frac{\alpha\alpha_0^2}{\lambda_c\varepsilon_l}$ for $\delta = 0.1$ $(\frac{\alpha\alpha_0^2}{\lambda_c\varepsilon_l} < 0)$ and $\delta = 0.1 + \pi$ $(\frac{\alpha\alpha_0^2}{\lambda_c\varepsilon_l} > 0)$.

TABLE III. Gray soliton solutions for some points in Fig. 6.

| $\delta$ | $\frac{\alpha\alpha_0^2}{\lambda_c\varepsilon_l}$ | $A_0$ | $A_1$ | $e^{-r}$ | $HW$ | $\frac{3}{2}\frac{\alpha\alpha_0^2}{\lambda_c\varepsilon_l}\frac{d}{\alpha_0}\frac{1}{\sin\delta}$ |
|---|---|---|---|---|---|---|
| 0.1 | −0.0186 | 0.9991 | 0.0988 | 0.8311 | 8.26 | 0.0874 |
| 0.1 | −0.0074 | 0.9996 | 0.0683 | 0.8797 | 11.69 | 0.0606 |
| 0.1 | −0.0025 | 1.000 | 0.0332 | 0.9332 | 21.23 | 0.0356 |
| $0.1+\pi$ | 0.0186 | 0.9991 | 0.0988 | 0.8311 | 8.26 | 0.0874 |
| $0.1+\pi$ | 0.0074 | 0.9996 | 0.0683 | 0.8797 | 11.69 | 0.0606 |
| $0.1+\pi$ | 0.0025 | 1.000 | 0.0332 | 0.9332 | 21.23 | 0.0356 |

$(-0.00, -0.024)$ linear mode is seen to have two minima in the barrier, which evolve into the two-dip wave function observed at $(\frac{\alpha}{\varepsilon_l}t^2,\lambda') = (-0.004, -0.0295)$. The point $(\frac{\alpha}{\varepsilon_l}t^2,\lambda') = (-0.004, -0.0295)$ is the linkage point of the branch of soliton modes that have just been discussed with the line of modes arising from $(\frac{\alpha}{\varepsilon_l}t^2,\lambda') = (-0.00, -0.024)$. At this point, the dark soliton modes along the linkage have been compressed to the extent that the barrier fits two dark soliton modes, and $(\frac{\alpha}{\varepsilon_l}t^2,\lambda') = (-0.004, -0.0295)$ is such a two dark soliton resonance. The widths of the two solitons are consistent with the results, 2.22, for the soliton widths found in Fig. 4. Continuing along the $(\frac{\alpha}{\varepsilon_l}t^2,\lambda') = (-0.00, -0.024)$ branch with increasing nonlinearity, amplitude results are presented for $(\frac{\alpha}{\varepsilon_l}t^2,\lambda') = (-0.005, -0.0315)$, which are consistent with the two-soliton nature of the barrier resonances along this branch.

### 2. *Gray solitons*

The solutions for gray solitons in the uniform infinite chain are given in the Appendix. Figure 6 presents results from these solutions for the width of the gray soliton dip region versus $\frac{\alpha\alpha_0^2}{\lambda_c\varepsilon_l}$ for $\delta = 0.1$ and $\delta = 0.1 + \pi$. Here, for a comparison with the barrier-scattering results, we take $\alpha_0 = t$. Table III also presents some of the wave functions and half-widths characterizing the gray soliton system in Fig. 6.

In general, it is seen that for a given $\frac{\alpha\alpha_0^2}{\lambda_c\varepsilon_l}$, the half-width of the gray soliton is larger than that of the dark soliton solutions and large on the scale of the barriers we have considered. As a consequence of this, for the cases of the barrier of five and nine sites, the gray solitons cannot be found in the regions plotted in Fig. 2, and the intensity dips arise solely from dark soliton resonances in the barrier. Larger barriers are needed for their observation. These will be a future consideration.

## IV. CONCLUSIONS

The solitonlike excitations in a nonlinear difference equation of an SRR chain[4,15,20,26] are investigated for barrier scattering. A mapping of the occurrence of the resonant-scattering maxima is presented in a two-dimensional space involving the barrier mutually inductive coupling and the barrier nonlinearity. The plot gives a rapid and effective demonstration of the properties of the barrier materials and the nature of the scattering expected as a function of position in the two-dimensional space.

This is an interesting problem as many systems exhibit equations of motion that are difference equations, e.g., lattice vibrations, magnetic systems, electron systems, photonic

crystals, etc. Systems that are described by difference equations of the same form (i.e., isomorphic) can exhibit similar types of solutions. These solutions may or may not be applicable to the system being described by the set of difference equations, depending on physical considerations. For example, the Maxwell Equations allow for both left- and right-handed wave solutions, but physical considerations of the parameters in the systems (i.e., the signs of the permittivity and permeability) are restricted in naturally occurring materials so that only right-handed waves are found. One must introduce artificial or engineered materials to make the left-handed wave solutions physically possible. Consequently, even though a set of equations are of the same abstract form, the parameters in the equations can restrict the set of solutions that are correct to the physical situation. If two physical systems are described by difference equations that are not of the same form (i.e., are not isomorphic), the set of solutions and their general forms can be different from one another. One set of equations can display solutions that the other cannot. For example, the linear media SRR difference equations considered in this paper do not exhibit the soliton solutions of the nonlinear media SRR difference equations considered in this paper. Consequently, the general form of difference equations can be used as a classification of the systems they describe. For example, the study presented here is similar to one we presented in Ref. 22 for a photonic-crystal waveguide of coupled resonators containing a barrier composed of Kerr nonlinear optical media and described by the one-dimensional difference equation[22–24]

$$E_l = \alpha[1+\lambda|E_l|^2]E_l + \beta|1+\lambda|E_{l+1}|^2|E_{l+1} + \beta[1+\lambda|E_{l-1}|^2]E_{l-1}. \quad (6)$$

Here, $E_l$ is the electric field at the $l$th site of the chain waveguide and the Greek characters are various parameters characterizing the waveguide. In that paper, the transmission resonances of a barrier of nonlinear optical media in a photonic-crystal waveguide were mapped out in a two-dimensional space involving parameters characterizing the linear and nonlinear parts of the dielectric interactions in the barrier media. Plots reminiscent to but different from those found in Fig. 2 were obtained and shown to exhibit lines of bright, dark, and multiple-pulse solitons. In this regard, notice that the dynamical difference equations in Eqs. (4b) and (6) are fundamentally different from one another (i.e., they are not isomorphic) and may be said to represent two general classes of distinct nonlinear difference equations. Equation (6) has nonlinearity on both the onsite and between-site couplings, while Eq. (4b) has nonlinearity only on the onsite coupling. These differences in the two sets of equations lead to fundamentally different behaviors in the two systems. This is an example of how the behaviors of different nonlinear systems can be characterized and classified by the nature of the nonlinearity present in their difference equations of motions.

While Eq. (6) has many branches of bright, multiple bright, and dark solitons in a two-dimensional plot of the scattering resonances arising from both large and small nonlinearities, Eq. (4b) shows only soliton and multiple soliton excitations near the small nonlinearity side of the two-dimensional plots in Fig. 2. For the small between-site couplings in our Eq. (4b) system, the dark soliton quickly breaks up into dips with small widths on the lattice and are not interesting. The reason for the limited range of solitons in the system of Eq. (4b) is that as the nonlinear interaction increases, the system in Eq. (4b) is overwhelmed by the onsite nonlinearity. The system in Eq. (6), however, maintains an increase in both the onsite and between-site interactions. This facilitates a variety of soliton behaviors in Eq. (6) throughout its plot in the two-dimensional space of transmission resonances. These behaviors are not observed in Eq. (4b).

In addition, we have presented in the Appendix various new results for the soliton modes in the infinite chain of SRR that were not treated in our previous work.[20] These include the dark and gray soliton solutions of the discrete uniform infinite chain and some of their continuum limiting forms. The discrete and continuum forms were compared and matched to one another. The half-widths of the bright, dark, and gray solitons were computed, and some analytic forms for them are given.

As a final point, it should be noted that we have chosen to study a model which has been the focus of a number of past studies of magneto-inductive and soliton modes, and we have taken parameters used in those past studies.[4,5,15,20,25] For this model, discussions have been given in the literature of the dissipative losses and of further than nearest-neighbor mutually inductive couplings. The problem of dissipation in these systems has in the past been addressed,[15] and it can be shown that the radiative and resistive losses are low enough for the easy observation of the various magneto-inductive and soliton modes that have been and are now studied. For instance, in Ref. 15, an experimentally realizable system is treated and found to have a rate of decay $\gamma = 0.0016$, yielding a time-dependent decay of the wave-function amplitude (computed in our paper; Ref. 20 on the model treated here) of $e^{-\gamma\tau/2}$. The transmission resonances of the barrier model we are studying are analogous to those found in the quantum mechanical problem of the transmission of a particle through a finite barrier. In our system, as with the quantum mechanics problem, the resonances come from the difference in barrier material, and they are not from resonances of the dielectric constants, which would require the development of an imaginary part of the dielectric. As a consequence, the wave-function losses in the linear chain and in the nonlinear barrier can both be limited by the discussions given above in this paragraph, referencing the work in Ref. 15. In regard to further than nearest-neighbor couplings, Eleftheriou, Lazarides, and Tsironis discussed these in Ref. 4, and discussions are found in the references given in Ref. 4. In Ref. 4, a treatment is given of the soliton excitations of the one-dimensional model we have taken in our studies. The authors of Ref. 4 found that for the weak couplings of interest to us, nearest-neighbor interactions give a good description of the system properties.

As mentioned earlier, it is hoped that the results presented for the two general forms of dynamical difference equations[4,20,22–24,27–31] in Eqs. (4b) and (6) will be extended to magnons, phonons, and electrons systems described by equations that are of isomorphic forms. In this regard, there has been some recent work on solitons in nanosystems[36–38] of a different type than ours, which can be similarly studied.

## ACKNOWLEDGMENT

The author wishes to thank the Department of Physics and Astronomy at University of California, Riverside, for the use of its library facilities.


## APPENDIX

### 1. Discrete uniform infinite chain

For a uniform infinite chain described by Eq. (1), within the RWA, there are three important types of solitonlike modes, including stationary breathers of the bright, dark, and gray types. Stationary breathers have wave functions separable in space and time coordinates, with $e^{-i\omega\tau}$ time dependence. For these modes, Eq. (1) in the RWA becomes

$$-\omega^2[q_n + \lambda_c(q_{n+1} + q_{n-1})] + q_n - \left(\frac{3\alpha}{\varepsilon_l}\right)|q_n|^2 q_n = 0 \tag{A1}$$

#### a. Bright-type modes

Two types of stationary bright discrete breathers are encountered. These were treated in Ref. 20 and are summarized here. One is a pulse centered at $n = 0$ of the form $q_0 = \alpha_0$ and $q_n = \alpha_0 A e^{-(|n|-1)r}$ for $n \neq 0$. The other is a pulse centered at $n = 0$ of the form $q_0 = \alpha_0$ and $q_n = \alpha_0(-1)^n A e^{-(|n|-1)r}$ for $n \neq 0$. Following the method of Sievers *et al.*,[30–33] the parameters $A, r$, and $\omega$ are determined as functions of the pulse height, $\alpha_0$, by choosing them to satisfy Eq. (A1) for $n = 0$, 1, and $n \to \infty$. The three nonlinear equations for $A$,$r$, and $\omega$ are

$$\frac{3\alpha}{\varepsilon_l}\alpha_0^2 \pm 2\lambda_c A \mp 2\lambda_c\left[1 - \frac{3\alpha}{\varepsilon_l}\alpha_0^2\right]\cosh(r) = 0, \tag{A2a}$$

$$\lambda_c(1 + Ae^{-r}) \pm \frac{3\alpha}{\varepsilon_l}\alpha_0^2 A^3 - 2\lambda_c\left[A - \frac{3\alpha}{\varepsilon_l}\alpha_0^2 A^3\right]\cosh(r) = 0, \tag{A2b}$$

and

$$\omega^2 = [1 \pm 2\lambda_c \cosh(r)]^{-1}, \tag{A2c}$$

where the upper (lower) signs are for the first (second) type of pulse forms given above. Notice that the linearly independent set $\{n^{m-1} A_m e^{-(|n|-1)r}\}$, where $m$ ranges over the integers, can be used to obtain a pulse solution that satisfies Eq. (A1) at all sites along the chain.[32] Here, only the first,$m = 1$, term of the series is needed in our discussions, and in this approximation the half-width of the pulse, $HW$, is given by $HW = 1 + \frac{\ln[2A]}{r}$.

Some of the general solutions of Eq. (A2) were discussed in Ref. 20. For the purposes of this paper, in Table I and Figs. 3(b) and 3(c), additional results are presented for bright soliton modes treated in the discussions of the barrier problem in the text. Table I presents the mode frequency, $\omega$, and $q_n$ for $n = 0$, 1, 2 as functions of $\lambda_c$, $\frac{\alpha}{\varepsilon_l}$, and $\alpha_0$. Figures 3(b) and 3(c) continue this comparison to the wave functions of some of the modes of the barrier resonances. The wave functions are seen to be sharply peaked along the chain, in accord with the assumptions of Eq. (A2).

#### b. Dark and gray-type modes

Dark and gray-type soliton modes are investigated in the discrete model by assuming trial solutions of the form[33–35]

$$q_0 = id, \tag{A3a}$$

$$q_n = \{\alpha_0(1 - A_0 e^{-nr} - nA_1 e^{-nr}) + id\}e^{in\delta}, \tag{A3b}$$

and

$$q_{-n} = -\{\alpha_0(1 - A_0 e^{-nr} - nA_1 e^{-nr}) - id\}e^{-in\delta}, \tag{A3c}$$

for $n > 0$. These are based on the continuum limits discussed later and on forms proposed in Refs. 20, 34, and 35. Here $\{n^m A_m e^{-nr}\}$ for integers, $m > 0$, is a linearly independent set with appropriate soliton boundary conditions that can be used to express the complete solution.[29] Only the first two members in this set are needed in the later discussions. Substituting Eq. (A3) into Eq. (A1) for $n = 0$, 1, 2, and $n \to \infty$, we find

$$-\omega^2[1 + 2\lambda_c \cos\delta] + 1 - \frac{3\alpha}{\varepsilon_l}\left(d^2 + \alpha_0^2\right) = 0, \tag{A4a}$$

$$\left[-\omega^2(1 + 2\lambda_c \cos\delta) + 1 - \frac{3\alpha}{\varepsilon_l}d^2\right]d - 2\lambda_c\omega^2\alpha_0 \sin\delta[1 - (A_0 + A_1)e^{-r}] = 0, \tag{A4b}$$

$$-\omega^2\{(1 + 2\lambda_c \cos\delta)d + \lambda_c\alpha_0 \sin\delta[A_0 + A_1 - (A_0 + 3A_1)e^{-2r}]e^{-r}\} + \left\{1 - \frac{3\alpha}{\varepsilon_l}\left[\alpha_0^2(1 - (A_0 + 2A_1)e^{-2r})^2 + d^2\right]\right\}d = 0, \tag{A4c}$$

$$-\omega^2\{(1 + 2\lambda_c \cos\delta)d + \lambda_c\alpha_0 \sin\delta[1 - (A_0 + 2A_1)e^{-2r}]\} + \left\{1 - \frac{3\alpha}{\varepsilon_l}\left[\alpha_0^2(1 - (A_0 + A_1)e^{-r})^2 + d^2\right]\right\}d = 0, \tag{A4d}$$

$$-\omega^2\{1 - (A_0 + A_1)e^{-r} + \lambda_c \cos\delta[1 - (A_0 + 2A_1)e^{-2r}]\} + \left\{1 - \frac{3\alpha}{\varepsilon_l}\left[\alpha_0^2(1 - (A_0 + A_1)e^{-r})^2 + d^2\right]\right\}[1 - (A_0 + A_1)e^{-r}] = 0, \tag{A4e}$$

and

$$-\omega^2\{1 - (A_0 + 2A_1)e^{-2r} + \lambda_c \cos\delta[2 - (A_0 + A_1)e^{-r} - (A_0 + 3A_1)e^{-3r}]\} + \left\{1 - \frac{3\alpha}{\varepsilon_l}\left[\alpha_0^2(1 - (A_0 + 2A_1)e^{-2r})^2 + d^2\right]\right\}[1 - (A_0 + 2A_1)e^{-2r}] = 0, \tag{A4f}$$

giving $A_0$, $A_1$, $e^{-r}$, $\alpha$, and $\omega^2$ as functions of $\alpha_0$, $\delta$, and $\lambda_c$. For $|\lambda_c|, |\frac{3\alpha\alpha_0^2}{\varepsilon_l}| \ll 1$ and retaining only terms linear in $\lambda_c$ and $\frac{3\alpha\alpha_0^2}{\varepsilon_l}$, these simplify to the following six nonlinear equations:

$$\omega^2 = 1 - \lambda_c\left[2\cos\delta + \frac{3\alpha\alpha_0^2}{\lambda_c\varepsilon_l}\left(1 + \frac{d^2}{\alpha_0^2}\right)\right], \tag{A5a}$$

$$\frac{3\alpha\alpha_0^2}{\lambda_c\varepsilon_l}\frac{d}{\alpha_0} - 2\sin\delta[1 - (A_0 + A_1)e^{-r}] = 0, \tag{A5b}$$

$$\frac{3\alpha\alpha_0^2}{\lambda_c\varepsilon_l}\frac{d}{\alpha_0}e^{-r}[-2 + (A_0 + 2A_1)e^{-2r}](A_0 + 2A_1) + \sin\delta[A_0 + A_1 - (A_0 + 3A_1)e^{-2r}] = 0, \tag{A5c}$$

$$\frac{3\alpha\alpha_0^2}{\lambda_c\varepsilon_l}\frac{d}{\alpha_0}e^{-r}[-2(A_0 + A_1) + (A_0 + A_1)^2e^{-r}] + \sin\delta[1 - (A_0 + 2A_1)e^{-2r}] = 0, \tag{A5d}$$

$$\frac{3\alpha\alpha_0^2}{\lambda_c\varepsilon_l}e^{-r}[-2 + 3(A_0 + A_1)e^{-r} - (A_0 + A_1)^2e^{-2r}](A_0 + A_1) + \cos\delta[-1 + 2(A_0 + A_1)e^{-r} - (A_0 + 2A_1)e^{-2r}] = 0, \tag{A5e}$$

and

$$\frac{3\alpha\alpha_0^2}{\lambda_c\varepsilon_l}e^{-r}[-2 + 3(A_0 + 2A_1)e^{-2r} - (A_0 + 2A_1)^2e^{-4r}](A_0 + 2A_1) + \cos\delta[-(A_0 + A_1) + 2(A_0 + 2A_1)e^{-r} - (A_0 + 3A_1)e^{-2r}] = 0, \tag{A5f}$$

giving $A_o$, $A_1$, $e^{-r}$, $\frac{d}{\alpha_0}$, $\frac{3\alpha\alpha_0^2}{\lambda_c\varepsilon_l}$, and $\omega^2$ as functions of $\alpha_0$, $\sin\delta$, and $\lambda_c$. We first consider the easier case of the dark soliton solutions of Eq. (A5), followed by a treatment of gray soliton solutions.

For dark solitons (i.e., $d = 0$, $\sin\delta = 0$), we take $d = 0$, $A_1 = 0$, and $\delta = 0$ in Eq. (A3). Proceeding as in the derivation of Eq. (A4), we find

$$-\omega^2[1 \pm 2\lambda] + 1 - \frac{3\alpha}{\varepsilon_l}\alpha_0^2 = 0, \tag{A6a}$$

$$-\omega^2\{1 - A_0e^{-r} \pm \lambda_c[1 - A_0e^{-2r}]\} + \left\{1 - \frac{3\alpha}{\varepsilon_l}\alpha_0^2(1 - A_0e^{-r})^2\right\}(1 - A_0e^{-r}) = 0, \tag{A6b}$$

and

$$-\omega^2\{1 - A_0e^{-2r} \pm \lambda_c[2 - A_0(e^{-r} + e^{-3r})]\} + \left\{1 - \frac{3\alpha}{\varepsilon_l}\alpha_0^2(1 - A_0e^{-2r})^2\right\}(1 - A_0e^{-2r}) = 0, \tag{A6c}$$

giving $A_0$, $e^{-r}$, and $\omega^2$ as functions of $\varepsilon_l$, $\alpha_0^2$, and $\lambda_c$. Here the upper signs are for the wave-function form $q_0 = 0$, $q_n = \alpha_0(1 - A_0e^{-r}) = -q_{-n}$, where $n > 0$, and the lower signs are for the wave-function form $q_0 = 0$, $q_n = (-1)^n\alpha_0(1 - A_0e^{-r}) = -q_{-n}$, where $n > 0$. In the limit of $|\frac{3\alpha}{\varepsilon_l}\alpha_0^2|$, $|\lambda_c| \ll 1$, retaining only terms linear in $\frac{3\alpha}{\varepsilon_l}\alpha_0^2$ and $\lambda_c$, these three nonlinear equations become

$$\omega^2 = 1 \mp \lambda_c\left[2 \pm \frac{3\alpha\alpha_0^2}{\lambda_c\varepsilon_l}\right], \tag{A7a}$$

$$\pm\frac{3\alpha\alpha_0^2}{\lambda_c\varepsilon_l}(-2 + A_0e^{-r})(1 - A_0e^{-r})A_0e^{-r} - 1 + 2A_0e^{-r} - A_0e^{-2r} = 0, \tag{A7b}$$

and

$$\pm\frac{3\alpha\alpha_0^2}{\lambda_c\varepsilon_l}(-2 + A_0e^{-2r})(1 - A_0e^{-2r})A_0e^{-2r} - A_0e^{-r} + 2A_0e^{-2r} - A_0e^{-3r} = 0, \tag{A7c}$$

giving $A_0$, $e^{-r}$, and $\omega^2$ as functions of $\frac{3\alpha\alpha_0^2}{\lambda_c\varepsilon_l}$. In the case that $|e^{-r}| \ll 1$ and $\frac{3\alpha\alpha_0^2}{\lambda_c\varepsilon_l}e^{-r}$ is of order 1, limiting forms for the solution of Eq. (A7) are

$$A_0 \cong 1, \tag{A8a}$$

$$e^{-r} \cong \mp\frac{1}{2\frac{3\alpha\alpha_0^2}{\lambda_c\varepsilon_l}}, \tag{A8b}$$

and

$$\omega^2 \cong 1 \mp \lambda_c\left[2 \pm \frac{3\alpha\alpha_0^2}{\lambda_c\varepsilon_l}\right]. \tag{A8c}$$

In Fig. 7, general results for $|\lambda_c| \ll 1$ dark solitons are presented from the numerical solution of Eq. (A7). Figure 7(a) shows a plot of $A_0$ versus $\frac{\alpha\alpha_0^2}{\lambda_c\varepsilon_l}$. The limiting form $A_0 \approx 1$ in Eq. (A8a) is found to be a good approximation over most of the plotted region. In Fig. 7(b), $x = e^{-r}$ is presented, giving the rate at which the kink approaches its asymptotic limiting values at the ends of the infinite chain. Again the approximation (dashed lines in the plot) in Eq. (A8b) is found to give a good representation of the solutions for most of the shown data. Figure 7(c) presents the dispersion using the full form $\omega^2 = (1 - \frac{3\alpha\alpha_0^2}{\varepsilon_l})/[1 + 2\lambda_c]$.

The half-width of the wave function envelopes as a function of $\frac{\alpha\alpha_0^2}{\lambda_c\varepsilon_l}$ is given in Fig. 4 for both the results from Eq. (A7) and the continuum limits discussed later. In our definition of the half-width for the results from Eq. (A7), we consider the general dark soliton envelope to be given

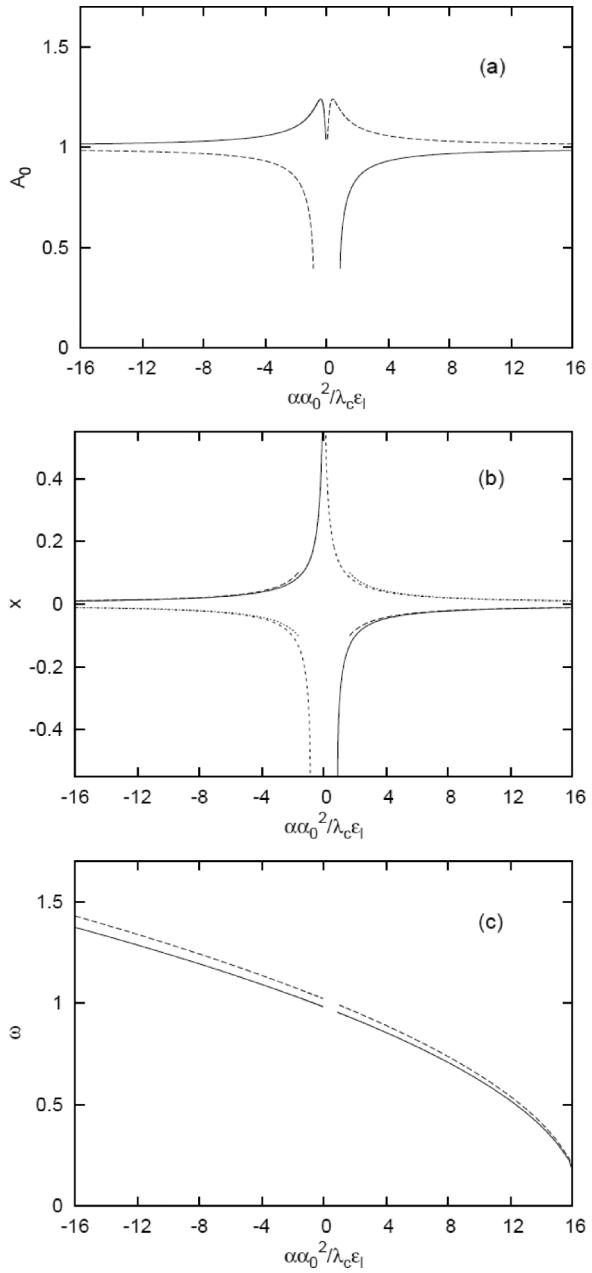


FIG. 7. Dark soliton results for the infinite chain from Eq. (A7). Plots as functions of $\frac{\alpha\alpha_0^2}{\lambda_c\varepsilon_l}$ are made for (a) $A_0$ where the solid (dashed) lines are the upper (lower) signs in Eq. (A7) and the asymptotic form $A_0 \approx 1$ is given in Eq. (A8a); and (b) $x = e^{-r}$ [solid line for the upper sign in Eq. (A7) and small dashed line for the lower sign in Eq. (A7)] with an asymptotic form $x \approx \mp 1/(6\frac{\alpha\alpha_0^2}{\lambda_c\varepsilon_l})$ (dashed and dotted lines ending near the center of the plot) given in Eq. (A8b); and (c) $\omega_\pm = \sqrt{\frac{1-\frac{3\alpha}{\varepsilon_l}\alpha_0^2}{1+2\lambda_c}}$. The upper (lower) dashed (solid) curve is for negative (positive) $\lambda_c$. Notice that in Fig. 7(c), the break in the plot around $\frac{\alpha\alpha_0^2}{\lambda_c\varepsilon_l} = 0$ comes because we only considered solutions of our system in the regions above and below the region of break.

by $q_n = \alpha_0(1 - A_0 e^{-nr})$ and allow $n$ to be extended to the real numbers. A definition of the half-width of the dark region of the wave function can then be given as the solution of $n$ from the equation $1 - A_0 e^{-nr} = \tanh(1)$. Here $\tanh(1)$ arises from the wave-function envelope of the continuum limit solution of the dark soliton, discussed below in Appendix Sec. B.

Gray soliton (i.e.,$d \neq 0$, $\sin\delta \neq 0$) solutions are obtained from Eq. (A5), which yields $A_0$, $A_1$, $e^{-r}$, $\frac{3\alpha\alpha_0^2}{\lambda_c\varepsilon_l}\frac{d}{\alpha_0}\frac{1}{2\sin\delta} = [1 - (A_0 + A_1)e^{-r}]$, the half-width of the soliton in units of the lattice constant as $HW = \frac{\ln[(A_0+A_1)/(1-\tanh(1))]}{-\ln[e^{-r}]}$, and the dispersion $\omega^2 = 1 - \lambda_c[2\cos\delta + \frac{3\alpha\alpha_0^2}{\lambda_c\varepsilon_l}(1 + \frac{d^2}{\alpha_0})]$ in terms of $\frac{\alpha\alpha_0^2}{\lambda_c\varepsilon_l}$. For the definition of the half-width of the gray soliton, we have applied the same reasoning as that for the dark soliton half-widths, taking $1 - [A_0 + A_1]e^{-nr} = \tanh(1)$ as the defining condition of the half-width of the amplitude dip. Of particular interest to us is the half-width that is presented in Fig. 6 for the case in which $\delta = 0.1$. It is seen that for fixed $\frac{\alpha\alpha_0^2}{\lambda_c\varepsilon_l}$, the widths of the gray solitons are much larger than those of the dark solitons. In Table III, results for the wave functions and their characteristics are plotted for some representative cases from Fig. 6.

### 2. Continuum limits of the infinite chain

The soliton solutions of the discrete system presented above can be matched up with their corresponding solutions in the continuum limits of Eqs. (1) and (A1), given by Eqs. (2) and (3). The continuum limits provide good qualitative descriptions of many of the soliton properties even in cases where the assumptions of the continuum limit do not apply.

#### *a. Pulse-breather modes*

A continuum limit solution of Eq. (2) for a stationary bright breather mode is given by[20]

$$q(x,\tau) = \sqrt{\frac{2\varepsilon_l[1-(1+2\lambda_c)\omega^2]}{3\alpha}} \times \operatorname{sech}\left\{\left[\frac{1-(1+2\lambda_c)\omega^2}{\lambda_c\omega^2}\right]^{1/2} x\right\} \exp[-i\omega\tau]. \tag{A9}$$

Expressing the sech-function argument in Eq. (A9) in terms of the pulse amplitude $q_0 = \sqrt{\frac{2\varepsilon_l[1-(1+2\lambda)\omega^2]}{3\alpha}}$, we find $[\frac{1-(1+2\lambda)\omega^2}{\lambda\omega^2}]^{1/2} = [\frac{3}{2}\frac{\alpha q_0^2}{\lambda\varepsilon_l}\frac{1}{\omega^2}]^{1/2}$. Treating $q_0$ as a variable and taking the $q_0$, $\lambda$, $\frac{\alpha}{\varepsilon_l}$, and $\omega^2$ values in Table I then gives a reasonable agreement between Eq. (A9) and the discrete model data in Table I for $q_1$ and $q_2$.

For the stationary pulse-breather modes, the continuum limit Eq. (3) was shown to have a solution of the form:

$$q(x,\tau) = \sqrt{\left|\frac{\varepsilon_l}{\alpha}\right|} a_0 \operatorname{sech}\{\beta x\} \exp[-i\omega\tau], \tag{A10}$$

where $\beta^2 = \frac{3}{2}\frac{\alpha\alpha_0^2}{a\varepsilon_l}$ and the pulse amplitude is $\alpha_0 = \sqrt{|\frac{\varepsilon_l}{\alpha}|}a_0$. Using the values for $\alpha_0$, $\lambda_c$, $\frac{\alpha}{\varepsilon_l}$, and $\omega^2$ in Table I, we find that Eq. (A10) gives a reasonable fit to the discrete model data in Table I for $q_0$, $q_1$, and $q_2$. This again is well outside the region of validity of the continuum limit. Both Eqs. (A9) and (A10), which are based on different limiting processes, yield

similar forms for the dependence of the pulse width on $\frac{\alpha}{\lambda_c \varepsilon_l}$ and the pulse amplitude. This is most likely indicative of the dependence on these variables in general.

### b. Gray and dark solitons

For the continuum limit given by Eq. (2), gray solitons exist and are of the form $q(x,\tau) = [A\tanh(Bx - C\tau) + iD]e^{i(kx-\omega\tau)} + cc$ for $D \neq 0$. This yields at $C = 0$ a stationary breather solution with

$$B^2 = -\frac{3}{2}\frac{\alpha}{\varepsilon_l}\frac{1}{\lambda_c\omega^2}A^2, \tag{A11a}$$

$$D = \frac{2}{3}\frac{\varepsilon_l}{\alpha}\lambda_c\omega^2 k\frac{B}{A}, \tag{A11b}$$

and

$$\omega^2 = \frac{1 - \frac{3\alpha A^2}{\varepsilon_l}}{1 + 2\lambda_c - 3\lambda_c k^2}. \tag{A11c}$$

In addition, results for the dark soliton solutions (i.e., $D = 0$) of Eq. (2) are found in Ref. 20 and agree with the $k = 0$ limit of Eq. (A11). Combining Eqs. (A11a) and (A11b), we find

$$\frac{3}{2}\frac{\alpha A^2}{\lambda_c\varepsilon_l}\frac{D}{A}\frac{1}{k} = \omega^2 B = \frac{\omega^2}{HW}, \tag{A11d}$$

where $HW$ is the half-width of the gray soliton. Taking $\omega^2 \approx 1$ and using the $HW$ values in Table III, we find that $\frac{3}{2}\frac{\alpha A^2}{\lambda_c\varepsilon_l}\frac{D}{A}\frac{1}{k} = 0.122, 0.086$, and $0.047$ for $\frac{\alpha\alpha_0^2}{\lambda_c\varepsilon_l} = 0.0186, 0.0074$, and $0.0025$, respectively. Even though the results of the discrete model are outside the range of validity of the continuum limit, the continuum limit form is in reasonable agreement with the results for the discrete mode in the last column of Table III.

In Ref. 20, only the bright and dark envelope and pulse-soliton solutions of the nonlinear Klein-Gordon equation in Eq. (3) were discussed. These are extended here to include gray soliton solutions of the nonlinear Klein-Gordon equation. The gray solitons of Eq. (3) are of the form

$$q(x,\tau) = \sqrt{\left|\frac{\varepsilon_l}{\alpha}\right|}a_0\left[\tanh\left(Bx - C\tau\right) + iD\right]e^{i(kx-\omega\tau)} + cc, \tag{A12}$$

where $a_0$, $B$, $C$, and $D$ are real coefficient, and we use the notation of Ref. 20. This mode differs from the dark soliton by the $iD$ term. Substituting Eq. (A12) into Eq. (3) and using the RWA to retain only terms in $e^{-i\omega\tau}$, we find

$$\omega^2 = b\left[1 - 3\frac{\alpha}{\varepsilon_l}\left|\frac{\varepsilon_l}{\alpha}\right|a_0^2(1 + D^2) + ak^2\right], \tag{A13a}$$

$$B = \frac{-\beta \pm \sqrt{\beta^2 + 4\alpha\gamma}}{2\alpha}, \tag{A13b}$$

and

$$C = \frac{1}{\omega}\left[abkB - \frac{3}{2}\frac{\alpha}{\varepsilon_l}\left|\frac{\varepsilon_l}{\alpha}\right|ba_0^2 D\right], \tag{A13c}$$

where

$$\alpha = a\left[ab\left(\frac{k}{\omega}\right)^2 - 1\right], \quad \beta = -3\frac{\alpha}{\varepsilon_l}\left|\frac{\varepsilon_l}{\alpha}\right|a_0^2 D\left(\frac{abk}{\omega^2}\right),$$

and

$$\gamma = \frac{3}{2}\frac{\alpha}{\varepsilon_l}\left|\frac{\varepsilon_l}{\alpha}\right|a_0^2\left[1 - \frac{3}{2}\frac{\alpha}{\varepsilon_l}\left|\frac{\varepsilon_l}{\alpha}\right|ba_0^2\frac{D^2}{\omega^2}\right].$$

In the $D \to 0$ limit, Eqs. (A12) through (A13) recover the dark soliton solution of Ref. 20. Taking soliton amplitude $\alpha_0 = \sqrt{|\frac{\varepsilon_l}{\alpha}|}a_0$, we find for the $C = 0$ gray soliton,

$$D = \frac{2}{3}\frac{\varepsilon_l}{\alpha}ak\frac{B}{\alpha_0^2}. \tag{A14}$$

Once the difference in the definitions $D$ in Eqs. (A11b) and (A14) are accounted for, these two formulations are in reasonable agreement for the dependence of $D$ on $B$ and the amplitude of the tanh envelope. In the limit in Eqs. (A12) and (A13) in which $C = 0$ and $D = 0$, the solutions become those of dark solition modes. For the dark soliton modes,

$$B^2 = \frac{3}{2}\frac{\alpha}{\varepsilon_l}\frac{\alpha_0^2}{a\left[ab\left(\frac{k}{\omega}\right)^2 - 1\right]} \tag{A15a}$$

and

$$\omega^2 = b\left[1 - 3\frac{\alpha}{\varepsilon_l}\alpha_0^2 + ak^2\right], \tag{A15b}$$

which are in reasonable agreement with the general forms of the dark soliton limit of Eq. (A11). In the limit that $|\lambda_c|, |\frac{\alpha\alpha_0^2}{\lambda\varepsilon_l}| \ll 1$, Eq. (A15a) becomes

$$B^2 = -\frac{3}{2}\frac{\alpha\alpha_0^2}{\lambda_c\varepsilon_l}, \tag{A16}$$

in agreement with the $k = 0$ dark soliton limit of Eq. (A11a). The half-width of the continuum soliton solutions are then defined from the $\tanh(Bx)$ form of the wave-function envelopes as $\frac{1}{B}$. This is seen in Fig. 4 to be in good agreement with the half-width computed from the theory in Eq. (A7). In making this comparison, the $\lambda_c \leftrightarrow -\lambda_c$ symmetry is invoked.

*arthur.mcgurn@wmich.edu

[1] D. R. Smith, W. J. Padilla, D. C. Vier, S. C. Nemat-Nasser, and S. Schultz, Phys. Rev. Lett. **84**, 4184 (2000).
[2] J. B. Pendry, A. J. Holden, D. J. Roberts, and W. J. Stewart, J. Phys.: Condens. Matter **10**, 4785 (1998).
[3] J. B. Pendry, A. J. Holden, D. J. Roberts, and W. J. Stewart, IEEE Trans. Microwave Theory Tech. **47**, 2075 (1999).
[4] M. Eleftheriou, N. Lazarides, and G. P. Tsironis, Phys. Rev. E **77**, 036608 (2008).
[5] G. V. Eleftheriades, Materials Today **12**, 30 (2009).
[6] E. Shamonina, V. A. Kalinin, K. H. Ringhofer, and L. Solymar, J. Appl. Phys. **92**, 6252 (2002).
[7] M. J. Freire, R. Marqués, F. Medina, M. A. G. Laso, and F. Martín, Appl. Phys. Lett. **85**, 4439 (2004).

[8]O. Sydoruk, O. Zhuromskyy, E. Shamonina, and L. Solymar, Appl. Phys. Lett. **87**, 072501 (2005).
[9]R. R. A. Syms, E. Shamonina, and L. Solymar, Eur. Phys. J.-B **46**, 301 (2005).
[10]A. A. Zharov, I. V. Shadrivov, and Y. S. Kivshar, Phys. Rev. Lett. **91**, 037401 (2003).
[11]S. O'Brien, D. McPeake, S. A. Ramakrishna, and J. B. Pendry, Phys. Rev. B **69**, 241101 (2004).
[12]M. Lapine, M. Gorkunov, and K. H. Ringhofer, Phys. Rev. E **67**, 065601 (2003).
[13]I. V. Shadrivov, S. K. Morrison, and Y. S. Kivshar, Opt. Express **14**, 9344 (2006).
[14]I. V. Shadrivov, A. N. Reznik, and Y. S. Kivshar, Physica B **394**, 180 (2007).
[15]I. Kourakis, N. Lazarides, and G. P. Tsironis, Phys. Rev. E **75**, 067601 (2007).
[16]Y. Tamayama, T. Nakanishi, and M. Kitano, Phys. Rev. B **87**, 195123 (2013).
[17]V. G. Veselago, Sov. Phys. Usp. **10**, 509 (1968).
[18]J. B. Pendry, D. Schurig, and D. R. Smith, Science **312**, 1780 (2006).
[19]V. M. Shalaev, Science **322**, 384 (2008).
[20]P. Giri, K. Choudhary, A. S. Gupta, A. K. Bandyopadhyay, and A. R. McGurn, Phys. Rev. B **84**, 155429 (2011).
[21]Y.-S. Lee, *Principles of Terahertz Science and Technology* (Springer, Berlin, 2009).
[22]A. R. McGurn, Phys. Rev. B **77**, 115105 (2008).
[23]A. R. McGurn, J. Phys.: Condens. Matter **20**, 025202 (2008).
[24]A. R. McGurn, J. Phys.: Condens. Matter **21**, 485302 (2009).
[25]R. W. Ziolkowski and N. Engheta, in *Metamaterials: Physics and Engineering Explorations*, edited by N. Engheta and R. W. Ziolkowski (IEEE Press, John Wiley and Sons, Inc., Hoboken, New Jersey, 2006), Chap. 1.
[26]N. N. Rosanov, N. V. Vysotina, A. N. Shatsey, I. V. Shadrivov, D. A. Powell, and Y. S. Kivshar, Opt. Express **19**, 26500 (2011).
[27]S. P. Shipman and S. Venakides, Nonlinearity **25**, 2473 (2012).
[28]S. P. Shipman, J. Ribbeck, K. H. Smith, and C. Weeks, IEEE Photon. J. **2**, 911 (2010).
[29]E. N. Bulgakov and A. F. Sadreev, Phys. Rev. B **80**, 115308 (2009).
[30]A. J. Sievers and J. B. Page, in *Dynamical Properties of Solids*, edited by G. K. Horton and A. A. Maradudin (North-Holland, 1995), p. 137.
[31]A. J. Sievers and S. Takeno, Phys. Rev. Lett. **61**, 970 (1988).
[32]A. J. Sievers and S. Takeno, Phys. Rev. B **39**, 3374 (1989).
[33]T. Dauxois and M. Peyrard, *Physics of Solitons* (Cambridge University Press, Cambridge, 2006), Chap. 3.
[34]A. R. McGurn, Phys. Lett. A **251**, 322 (1999).
[35]A. R. McGurn, Phys. Lett. A **260**, 314 (1999).
[36]R. E. Noskov, P. A. Belov, and Yu. S. Kivshar, Sci. Rep. **2**, 873 (2012).
[37]R. E. Noskov, P. A. Belov, and Yu. S. Kivshar, Phys. Rev. Lett. **108**, 093901 (2012).
[38]R. E. Noskov, P. A. Belov, and Yu. S. Kivshar, Opt. Express **20**, 2733 (2012).